Author version: *Geochem. Geophys. Geosyst., vol.13; 2012; 15pp, Q01009, doi:10.1029/2011GC003888*

Hydrothermal plumes over the Carlsberg Ridge, Indian Ocean

Durbar Ray[1], Kamesh Raju K. A.[1], Edward T. Baker [2], Srinivas Rao A. [1], Abhay V. Mudholkar[1], John E. Lupton [2], Surya Prakash L.[1], Rekha B. Gawas[1], Vijaya Kumar T[3]

[1]*CSIR-National Institute of Oceanography, Goa, India*
[2]*Pacific Marine environmental Laboratory, NOAA, USA*
[3]*CSIR-National Geophysical Research Institute, Hyderabad, India*

[1] Indian Ocean ridges north of the Rodriguez Triple Junction remain poorly explored for seafloor hydrothermal activity, with only two active sites confirmed north of 25°S. We conducted water column surveys and sampling in 2007 and 2009 to search for hydrothermal plumes over a segment of the Carlsberg Ridge. Here we report evidence for two separate vent fields, one near 3°42'N, 63°40'E and another near 3°41.5'N, 63°50'E, on a segment that is apparently sparsely magmatic. Both sites appear to be located on off-axis highs at the top of the southern axial valley wall, at depths of ~3600 m or shallower (~1000 m above the valley floor). At the 63°40'E site, plume sampling found local maxima in light scattering, temperature anomaly, oxidation-reduction potential (ORP), dissolved Mn, and ^{3}He. No water samples are available from the 63°50'E site, but it showed robust light-scattering and ORP anomalies at multiple depths, implying multiple sources. ORP anomalies are very short lived, so the strong signals at both sites suggest that fluid sources lie within a few kilometers or less from the plume sampling locations. Although ultramafic rocks have been recovered near these sites, the light-scattering and dissolved Mn anomalies imply that the plumes do not arise from a system driven solely by exothermic serpentinization (e.g., Lost City). Instead, the source fluids may be a product of both ultramafic and basaltic/gabbroic fluid-rock interaction, similar to the Rainbow and Logatchev fields on the Mid-Atlantic Ridge.

1. Introduction

[2] The Central Indian, Carlsberg, and Sheba ridges bisect the Indian Ocean from the Rodriguez Triple Junction at 25°S to the entrance of the Gulf of Aden at 15°N. Hydrothermal exploration has been sparse along this lengthy section of slow-spreading ridge, with most investigations concentrated at ridge segments south of ~18°S [*Gamo et al.,* 1996, 2001; *Van Dover et al.,* 2001; *Kawagucci et al.,* 2008]. Farther north, *Murton et al.* [2006] collected 12 light-scattering profiles and one CTD cast between 5°41'N and 9°58'N in 2003, finding evidence of a massive event plume, CR2003, between 5°41'N, 61°30'E and 6°20'N, 60°33'E. A series of CTD profiles in the same area a year later [*Ray et al.,* 2008] found evidence of a chronic hydrothermal plume. Neither study was able to provide any information about the location of seafloor vent sources. Other than these slim results, no other hydrothermal evidence has been reported from midocean ridges north of 18°S in the Indian Ocean.

[3] Exploration north of the Rodriguez Triple Junction has led to the discovery of only two active discharge sites: the Kairei field at 25°19.2'S, 70°2.4'E [*Hashimoto et al.,* 2001; *Gamo et al.,* 2001; *Van Dover et al.,* 2001], and the Edmond field at 23°52.7'S, 69°35.8'E [*Van Dover et al.,* 2001]. This meager total has profound implications for many aspects of hydrothermal research, most especially the biogeography of deep-sea vent fauna. Presently, six or seven global biogeographic provinces are recognized, sometimes including fauna from the Kairei and Edmond field as a separate province [*Van Dover et al.,* 2002; *Ramirez-Llodra et al.,* 2007], and sometimes including them with a western Pacific province [*Bachraty et al.,* 2009]. The paucity of available samples from the Indian Ocean is a major obstacle in resolving the role of the Indian Ocean ridges as migration corridors for hydrothermal vent fauna.

[4] Here we describe results from two expeditions designed to discover active hydrothermal venting on the Carlsberg Ridge. In 2007, a continuous water column survey from 62°20'E to 66°20'E identified hydrothermal plume signals between 63°30' and 64°E and collected plume samples using CTD casts. This area is ~370 km away from the CR-2003 event plume site [*Murton et. al.*, 2006]. A return cruise in 2009 conducted a dense array of vertical casts in the same area. These casts detected plumes with reduced hydrothermal chemicals in two areas separated by ~15 km. We thus have firm evidence of two active sites, with location precision sufficient to justify seafloor exploration with a manned or unmanned vehicle.

2. Geological setting of the survey area

[5] The Carlsberg Ridge in the northwest Indian Ocean defines the plate boundary between the Indian and Somalian plates [*McKenzie et al.,* 1970]. The Carlsberg Ridge begins at the Owen fracture zone near 10°N and extends to the Central Indian Ridge near the equator (Figure 1A). The Carlsberg Ridge is a typical slow-spreading ridge with an average half-spreading rate of 11 to 16 mm/yr, a V-shaped rift valley, and a wide valley floor. Segments are both magmatic and sparsely magmatic, and discontinuities are both non-transform discontinuities (NTDs) and well-defined transform faults (TFs) [*Kamesh Raju et al.,* 2008].

[6] The segmentation pattern of the Carlsberg Ridge between 62°20'E and 66°20'E (Figure 1A) has been investigated using swath bathymetry and magnetic data [*Kamesh Raju et al.,* 2008]. Swath bathymetry revealed rugged topography with steep valley walls, geo-morphological structures like ridge-parallel topographic fabric, and axial volcanic ridges. A mantle Bouguer anomaly low of ~50 mGal [*Kamesh Raju et. al.,* 1998] indicates focused mantle upwelling and thick crust underneath this propagating ridge section. Based on tectonic features and valley floor depths, we divided this ridge section into four segments (Figure 1A). Segment II (63°10' to 63°18'E) is the most distinctive segment. It has the widest (maximum width ~25 km) and the deepest (maximum depth ~4700 m) axial valley floor, and is characterized by blocky topographic fabric and off-axial highs (Figure 1B).

[7] Seabed samples dredged from different parts of Segment II consist mostly of fresh basalts; mantle-derived rocks such as peridotites and serpentinites were found at three locations (Figure 1A) [*Mudholkar et al.,* 2002; *Kamesh Raju et al.,* 2008]. The ultramafic rocks from the valley and flanks contain serpentine with large (~8-10 mm) ortho-pyroxene crystals [*Mudholkar et al.,* 2002], a hydrated product of olivine. Anorthosites, also of mantle origin and mostly composed of feldspar, were found in few samples. Such serpentinized ultramafics or mixture of basalts and ultramafic outcrops are commonly found in active hydrothermal fields over the slow and ultra-slow spreading Mid-Atlantic Ridge [*Rona et al.,* 1987; *Bougault et al.,* 1993; *Gracia et al.,* 2000; *Da Costa et al.,* 2008; *Marbler et al.,* 2010], Southwest Indian Ridge [*Bach et al.,* 2002] and Mid-Cayman Rise [*German et al.,* 2010]. Because of its anomalous geologic setting, we chose to explore Segment II for hydrothermal sites using detailed water column investigations.

3. Survey strategy and methods

[8] In December 2007, we used the *RV Sonne* (RVS-2 cruise) to conduct a continuous, 440-km-long tow through the rift valley between 62°20'E and 66°20'E. A combined seabed mapping and plume

survey was carried out using the IMI-30 deep-towed side-scan sonar system and Miniature Autonomous Plume Recorders (MAPRs). The deep water above the valley floor was surveyed using an array of six MAPRs clamped on the deep-tow (DT) cable (Figure 2), similar to other investigations combining side-scan sonar and MAPRs [e.g., *German et al.,* 1998; *Baker et al.,* 2008]. We also conducted a shorter deep-tow- MAPR (DT-06) survey along the top of the southern valley wall in the middle of Segment II (Figure 3). More precise hydrographic data and water samples were collected by vertical Conductivity-Temperature-Depth (CTD) casts. Our Seabird CTD (SBE 9/11 plus) system included duplicate light backscattering sensors (WET Labs 634) and 24 acid-washed Niskin bottles (capacity 10 l). Anomalies in potential temperature ($\Delta\theta$) were determined from corresponding relationships with potential density, σ_θ [*Lupton et al.,* 1985; *Baker and Massoth,* 1987; *Thomson et al.,* 1992]. Light backscattering is reported as nephelometric turbidity unit (NTU) [*American Public Health Association,* 1985]; ΔNTU is the difference in turbidity of plume water and ambient non-plume water.

[9] Seawater samples between 2500 and 4300 m were analyzed for dissolved manganese (DMn) and helium isotopes (^{3}He and ^{4}He), sensitive tracers for detecting hydrothermal fluids in the ocean [e.g., *Lupton et al.,* 1980]. Water samples for helium isotopes were collected in fresh copper tubes using the cold crimping method described by *Young and Lupton* [1983]. Helium isotopes were analyzed on a dual-collector noble gas mass spectrometer [*Lupton,* 1976] at the Helium Isotope Laboratory, NOAA/PMEL, Newport, Oregon, USA. The presence of excess dissolved ^{3}He in water samples is expressed as δ^3He(%)= (R/R_{atm}-1)X100, where R and R_{atm} represent the ^{3}He/^{4}He ratio in the seawater sample and the atmosphere respectively [*Lupton,* 1998]. The 1-sigma uncertainty in the ^{3}He/^{4}He ratio is about 0.2%. DMn in seawater was analyzed following the method described by *Danielsson et al.* [1978]. Onboard, seawater samples were filtered through 0.45 µm filters and acidified with ultra-pure HNO_3 to pH ~2.0. DMn was extracted using sodium dodecyle-dithio-carbamate, trihydrate (SDDC) and methyl-isobutyl-ketone (MIBK), and then back extracted in a 2.0% ultra-pure HNO_3 medium. Those extracted solutions were analyzed on a Graphite Furnace-AAS, at NIO, Goa, India with analytical precision of ~3.0%.

[10] Seawater samples were also collected for suspended particulate matter analyses. A 10 l seawater sample from each depth was filtered through a single 0.45 µm filter paper, rinsed with distilled water, dried, and kept in separate petriplates. Filtered particles were studied with a scanning electron microscope (SEM) and assessed for qualitative chemical composition with an energy dispersive X-Ray spectrometer (EDS).

[11] A second expedition to the same region was undertaken in April-May 2009, onboard *MV Akademik Boris Petrov* (BPR-1 cruise). During this survey, 23 MAPR hydrocasts were planned around the location where plume signatures were observed in 2007. No CTD casts or water sampling occurred during this expedition. In 2009, we used a new version of MAPRs equipped with an oxidation-reduction potential (ORP) sensor as well as the standard high-precision temperature and light back-scattering sensors. ORP values [*E* (mV)] are highly sensitive to short-lived reduced chemicals in hydrothermal plumes, such as Fe^{2+} and H_2S, and generally occur as a sharp decline in *E* followed by a gradual recovery [*Nakamura et al.,* 2000; *Walker et al.,* 2007; *Baker et al.,* 2010]. Unlike hydrographic, light backscattering, and many hydrothermal chemical (e.g., Mn, ^3He) anomalies, *E*-anomalies (ΔE) disappear quickly as reduced chemicals oxidize. Depending on local current speed, significant *E* drops are only observed within a radius of ~1.0 km of an active hydrothermal source [*Walker et al.,* 2007; *German et al.,* 2008], and so are especially valuable in determining source location.

4. Results and discussion

4.1. The 2007 cruise

[12] During the first expedition, the axial rift valley of four segments (Figure 1A) in the study area was investigated for plume signatures. ΔNTU values in the axial valley along Segments I, III and IV were minimal, but on DT-04 the shallowest MAPR detected a weak signal near 03°45.7'N, 63°37'E in Segment II. CTD casts at S6, S8, S9 and S10 (Figure 3) subsequently revealed a 100-150 m thick ΔNTU layer between 3200 and 3300 m (Figure 4). Because this plume was found 800-1000 m above the valley floor, its most likely source location was on an off-axis high on the rift valley wall. Based on these observations we conducted another deep-tow-MAPR track (DT-06, Figure 3) along the southern wall of the rift valley.

[13] DT-06 imaged a plume stretching from 63°39'E to 63°46'E, between 2900 m and 3300 m, with maximum ΔNTU anomalies of ~0.035 near 63°44.5'E (Figure 5). The constant plume height of ~200 m indicates that the particles originated from a hydrothermal source rather than by resuspension from the seafloor. Two CTD (with MAPR) casts (S16 and S17, Figures 3 and 5, Table 1) collected hydrographic data and water samples around the plume ΔNTU maximum. S17 showed a maximum ΔNTU of ~0.01 between 3000 and 3150 m (Figure 6F). This backscatter layer had average temperature anomaly, $\Delta\theta$, of ~0.005°C (Figure 6E). The plots of potential temperature, θ, versus potential density, σ_θ, (Figure 7A) and salinity (Figure 7B) of the water column at S17 clearly indicate the effluent layer between 3040 and 3200 m.

[14] We further verified the hydrothermal origin of this layer by analyzing seawater for DMn and He isotopes. Samples from the plume layer at both the CTD stations showed significant enrichment of DMn (2.4 - 2.7 nmoles/l, Table 2) relative to either the local background concentration (1.2±0.3 nmoles/l) or average Indian Ocean deep waters [0.08 to 1.8 nmoles/l, *Saager et al.,* 1989]. All water samples were also analyzed for He-isotopes, the most definitive chemical tracer for hydrothermal activity. Hydrothermal venting is considered to be the source of this excess ^{3}He in the deep ocean as part of the processes generating new oceanic crust [*Craig and Lupton,* 1981; *Jean-Baptiste et al.,* 2008]. Samples from the effluent layer of S17 have a small but distinct excess of ^{3}He (maximum $\delta^{3}He$ = 16.4%, ^{3}He = $6.8X10^{-14}$ cc STP/g at 3060 m, Table 2) compared to that in waters immediately above and below the effluent layer (Figure 6G). The $\delta^{3}He$-profile at CTD station S16 also had a consistent enrichment of ^{3}He (maximum $\delta^{3}He$=16.9%, ^{3}He=$6.9X10^{-14}$ cc STP/g at 3200 m) at the depths ranging between 3050 and 3200 m (Figure 6C, Table 2). The highest $\delta^{3}He$ value in the present study is slightly higher than in the surrounding waters ($\delta^{3}He$=14-15%) and also higher than values from earlier records of Indian Ocean deep water between the equator and 6°N [$\delta^{3}He$= 11 to 14%, *Srinivasan et al.,* 2004]. The overall vertical distribution of DMn and $\delta^{3}He$ co-vary and closely follow the ΔNTU and $\Delta\theta$ profiles at CTD S17 (Figure 6). CTD S16 exhibited a prominent increase in DMn and $\delta^{3}He$ but no detectable ΔNTU or $\Delta\theta$ signature.

[15] We used SEM to investigate suspended particulate matter collected from different depths on CTD S17 to identify the mineralogy as well as the chemistry of the particles. Filtered material from seawater immediately above (2600, 2800 and 2900 m) and below (3320 and 3400 m) the backscatter layer appeared as a uniform mass of extremely fine (~1.0 μm) particles, whereas material from the backscatter layer (3060 m) included several large (~40-300 μm) black particles in addition to fine particulates. SEM images of 16 of such large particles revealed that most of them have rough vesicular surfaces (Figures 8A to 8D) while the rest have a well-defined smooth, platy texture (Figures 8E and 8F).

[16] EDS results show that vesicular particles are quite rich in Si (SiO_2 ~49-73%), Fe (FeO ~9-15%), Al (Al_2O_3 ~2-13%) and Ca (CaO ~1.1%). Although it is difficult to identify such micron-sized particles based only on external texture and qualitative chemical composition, these particles are likely Fe-Mg-smectite or related clays, commonly found with hydrothermal sulfides [*Dekov et al.,* 2008] or sediments [*Fortin et al.,* 1998; *Lackschewitz,* 2006]. In contrast, particles with platy layers (Figures 8E and 8F) are enriched with Si (SiO_2 ~60%) and Mg (MgO ~32%) but low in Fe (FeO <0.9%). The composition of Mg-Si-rich particulates showed a molar ratio of Mg:Si:O::03:04:12. Therefore, based on texture and chemistry, we propose that these multi-layered particles are magnesium-silicate minerals, probably talc

($Mg_3Si_4O_{10}(OH)_2$), which normally forms by low-grade metamorphic changes in ultramafic rocks [Van *Gosen et al.*, 2004] during hydrothermal alteration. *Dymond and Roth* [1988] also identified talc and smectite particulates in hydrothermal plumes over the Endeavour segment of the Juan de Fuca Ridge.

4.2. The 2009 cruise

[17] During the 2009 cruise we conducted a series of MAPR hydrocasts around the 2007 track of DT-06 (Figure 3), concentrating on the location of maximum ΔNTU anomalies (Figure 5). Of 19 MAPR casts (stations 8 to 25 and 32), none showed a ΔNTU anomaly as intense as seen on S17 in 2007 and none showed an *E*-anomaly indicating a nearby source. Most anomalies appear as a broad ΔNTU increase below ~2900 m that corresponds to the depth of the 2007 plume (Figure 9).

[18] Four MAPR casts (36-39 in Figure 3) near the end of DT-06 track, however, all found robust ΔNTU plumes and distinct or subtle Δ*E* values, centered between 3100 m and 3400 m (Figure 10). Three casts detected ΔNTU anomalies greater than any seen in 2007. The largest Δ*E* (~5.0 mV) occurred at station 36 (03°41.72'N, 63°40.22'E); other casts showed weaker deflections or simply changes in the vertical gradient of *E*. Because the weakest ΔNTU and Δ*E* were at station 37, the most southeasterly of the four, we predict the source to be closer to the station 36-38-39 grouping. Conducting these four stations occupied ~24 hrs, and during that period the depth of the plume anomalies steadily shallowed. This variability was most likely caused by tidal-current-induced plume bending, as observed over the TAG field [*Rudnicki et al.*, 1994].

[19] In addition to our survey at the edge of an off-axis high at 63°40'E, we also made an exploratory cast (station 26) at a similar off-axis high at 63°50'E (Figure 3, Table 1). This MAPR station exhibited a complex profile with two prominent ΔNTU peaks at 2930 and 3120 m (Figure 11). The upper plume was shallower than any seen near 63°40'E, whereas the lower plume was in the same depth interval as those plumes. Both plumes showed clear Δ*E* anomalies, with the upper plume having the largest anomaly (Δ*E* ~17 mV) recorded during the entire cruise. The strength of the Δ*E* anomaly ensures that the corresponding seafloor source is on the 63°50'E promontory, distinct from the sources found near 63°40'E. The multi-plume profile also implies multiple sources in this area, either in the same vent field or at different locations.

4.3. Vent source possibilities

[20] The chemical and physical characteristics of the plumes over both off-axis highs provide important clues to the nature of the vent sources. At both sites, plumes have substantial ΔNTU and Δ*E*

anomalies. Chemical analysis of the 63°40'E plume also found clear anomalies in DMn. The ΔNTU and DMn anomalies indicate that the source fluids cannot be products of a vent system driven solely by the exothermic serpentinization of ultramafic rocks. At the type example for such systems, the Lost City field on the Mid-Atlantic Ridge, metal-free (and thus virtually particle-free) fluids of low temperature (<~75°C) form a low-rising, almost invisible plume [*Kelley et al.,* 2001]. These Carlsberg vents may be more similar to the Rainbow and Logatchev vent fields on the Mid-Atlantic Ridge. As with the plumes we discovered, those fields lie near the intersection of the axial valley and a non-transform discontinuity. At Rainbow and Logatchev, vent fluid chemistry and temperature points toward interaction with basaltic/gabbroic material as well as interaction with peridotite [*Janecky and Seyfried,* 1986*; Wetzel and Shock,* 2000; *Douville et al.,* 2002; *Schmidt et al.,* 2007; *Seyfried et al.,* 2011]. Both of these rock types have been collected within Segment II (Figure 1A) [*Kamesh Raju et al.,* 2008].

5. Conclusions

[21] We have identified hydrothermal plumes from unknown active vent(s) near 3°42'N, 63°40E and 3°41.5'N, 63°50E on the Carlsberg Ridge. Prominent optical backscatter and thermal anomalies coupled with chemical (e.g. ΔE, ^{3}He, Mn) signatures in seawater demonstrated the existence of hydrothermal sources on off-axis highs on the south wall of the Carlsberg Ridge. Pronounced backscatter anomalies and anomalous DMn concentrations suggest a high temperature hydrothermal source for the plume. The newly discovered submarine plumes have a maximum thickness of ~200 m and maximum rise height of about 400 m from seafloor, resembling a typical chronic hydrothermal plume rather than the apparent event plume discovered on the Carlsberg Ridge by *Murton et al.* [2006]. Pronounced ΔE anomalies imply that the vent field locations are within a radius of a few kilometers or less from the cast sites.

[22] The coincidence of ΔE and ΔNTU anomalies on cruises two years apart confirms active venting in the study area and is the first record of a chronic plume over the Carlsberg Ridge. The geographic specificity of the anomalies is enough to justify further investigations with autonomous under-water or remotely operated vehicles to locate the first active vent on the slow-spreading Carlsberg Ridge.

Acknowledgements

[23] We thank Dr. S. R. Shetye, Director, National Institute of Oceanography and Dr. Y. J. Bhaskar Rao, Director, National Geophysical Research Institute for their encouragement and continuous support. Thanks to the Masters, crew members, our scientific and technical colleagues onboard *RV Sonne* and *MV Akademik Boris Petrov* for their support during the cruises. Present investigation was

funded by CSIR under Network project COR-006 and MoES, Govt. of India, under Grant-in Aid project GAP-2157. Thanks to Mr. V. D. Khedekar for SEM-EDS analyses of particulate matter. We acknowledge the excellent support of Sharon Walker in providing MAPRs for the cruises. We also thank Ron Greene and Leigh J. Evans for analysis of helium isotopes in seawater samples. Authors are thankful to Dr. William Chadwick and an anonymous reviewer for their suggestions and constructive comments. This is NIO contribution number xxxx and PMEL contribution number 3740.

References

American Public Health Association (1985), Standard Methods for the Examination of Water and Wastewater, 16th ed., APHA, AWWA, and WPCF joint publication, 1268 pp., Washington, D. C.

Bach, W., N. R. Banerjee, H. J. B. Dick, and E. T., Baker (2002), Discovery of ancient and active hydrothermal systems along the ultra-slow spreading Southwest Indian Ridge 10° – 16°E, *Geochem. Geophys. Geosyst*, *3,* 1044, doi: 10.1029/2001GC000279.

Bachraty, C., P. Legendre, and D. Desbruy`eres (2009), Biogeographic relationships among deep-sea hydrothermal vent faunas at global scale, *Deep-Sea Res. I, 56,* 1371–1378.

Baker, E. T., and G. J., Massoth (1987), Characteristics of hydrothermal plumes from two vent fields on the Juan de Fuca Ridge, northeast Pacific Ocean, *Earth Planet. Sci. Lett., 85,* 59-73.

Baker, E. T., R. M. Haymon, J. A. Resing, S. M. White, S. L. Walker, K. C. Macdonald, and K. Nakamura (2008), High-resolution surveys along the hot spot-affected Galápagos Spreading Center: 1. Distribution of hydrothermal activity, *Geochem. Geophys. Geosyst., 9,* Q09003, doi: 10.1029/2008GC002028.

Baker, E. T., F. Martinez, J. A. Resing, S. L. Walker, N. Buck, and M. H. Edwards (2010), Hydrothermal cooling along the Eastern Lau Spreading Center: No evidence for discharge beyond the neovolcanic zone, *Geochem. Geophys. Geosyst., 11,* Q08004, doi: 10.1029/2010GC003106.

Bougault, H., J. L. Charlou, Y. Fouquet, H. D. Needham, N. Vaslet, P.,Appriou, P. Jean-Baptiste, P. A. Rona, L. Dmitriev, and S. Silantiev (1993), Fast and slow spreading ridges: structures and hydrothermal activity, ultramafic topographic highs, and CH_4 output, *J. Geophys. Res., 98,* 9643–9651.

Craig, H., and J. E. Lupton (1981), Helium-3 and mantle volatiles in the ocean and the oceanic crust. In: The Sea, vol. 7, pp. 391-428, C. Emiliani (ed), John Wiley & Sons. New York, USA.

DaCosta, I. R., F. J. A. S. Barriga, and R. N., Taylor (2008), Late seafloor carbonate precipitation in serpentinites from the Rainbow and Saldanha sites (Mid-Atlantic Ridge), *Europe. J. Mineral., 20,* 173-181.

Danielsson, L. G., B. Magnusson, and S. Westerlund (1978), An improved metal extraction procedure for the determination of trace metals in sea water by Atomic Absorption Spectrometry with electrothermal atomization, *Anal. Chim. Acta, 98,* 47 -57.

Dekov, V. M., J. Cuadros, W. C. Shanks, and R. A. Koski (2008), Deposition of talc—kerolite–smectite—smectite at seafloor hydrothermal vent fields: Evidence from mineralogical, geochemical and oxygen isotope studies, *Chem. Geol., 247,* 171-194.

Douville, E., J. L. Charlou, E. H. Oelkers, P. Bienvenu, C. F. Jove Colon, J. P. Donval, Y. Fouquet, D. Prieur, and P. Appriou (2002), The Rainbow vent fluids (36°14'N, MAR): the influence of ultramafic rocks and phase separation on trace metal content in Mid-Atlantic Ridge hydrothermal fluids, *Chem. Geol., 184,* 37-48.

Dymond, J., and S. Roth (1988), Plume dispersed hydrothermal particles: A time-series record of settling flux from the Endeavour Ridge using moored sensors, *Geochim. Cosmochim. Acta, 52,* 2525-2536.

Fortin, D., F. G. Ferris, and S. D. Scott (1998), Formation of Fe-silicates and Fe-oxides on bacterial surfaces in samples collected near hydrothermal vents on the Southern Explorer Ridge in the northeast Pacific Ocean, *Am. Mineral., 83,* 1399–1408.

Gamo, T., E. Nakayama, K. Shitashima, K. Isshiki, H. Obata, K. Okamura, S. Kanayama, T. Oomori, T. Koizumi, S. Matsumoto, and H. Hasumoto (1996), Hydrothermal plumes at the Rodriguez triple junction, Indian Ocean, *Earth Planet. Sci. Lett., 142,* 261-270.

Gamo, T., H. Chiba, T. Yamanaka, T. Okudaira, J. Hashimoto, S. Tsuchida, J. Ishibashi, S. Kataoka, U. Tsunogai, K. Okamura, Y. Sano, and R. Shinjo (2001), Chemical characteristics of newly discovered black smoker fluids and associated hydrothermal plumes at the Rodriguez Triple Junction, Central Indian Ridge, *Earth Planet. Sci. Lett., 193,* 371–379.

German, C. R., E. T. Baker, C. Mevel, K. Tamaki, and the FUJI Scientific Team (1998), Hydrothermal activity along the southwest Indian Ridge, *Nature*, *395,* 490 –493.

German, C. R., D. R. Yoerger, M. Jakuba, T. M. Shank, C. H. Langmuir, and K. Nakamura (2008), Hydrothermal exploration with the Autonomous benthic Explorer, *Deep Sea Res. -I*, *55,* 203-219.

German, C. R., A. Bowen, M. L. Coleman, D. L. Honig, J. A. Huber, M. V. Jakuba, J. C. Kinsey, M. D. Kurz, S. Leroy, J. M. McDermott, B Mercier de Lépinay, K. Nakamura, J. S. Seewald, J. L. Smith, S. P. Sylva, C. L. Van Dover, L. L. Whitcomb, and D. R. Yoerger (2010), Diverse styles of submarine venting on the ultraslow spreading Mid-Cayman Rise, *Proc. Nat. Acad. Sci.,107,* 14020-14025. doi: 10.1073/pnas.1009205107.

Gracia, E., J. L. Charlou, J. Radford-Knoery, and L. M. Parson (2000), Non-transform offsets along the Mid-Atlantic Ridge south of the Azores (38°N– 34°N): ultramafic exposures and hosting of hydrothermal vents, *Earth Planet. Sci. Lett., 177,* 89– 103.

Hashimoto, J., S. Ohta, T. Gamo, H. Chiba, T. Yamaguchi, S. Tsuchida, T. Okudaira, H. Watabe, T. Yamanaka, and M. Kitazawa (2001), First hydrothermal vent communities from the Indian Ocean discovered, *Zool. Sci. 18,* 717–721.

Janecky, D. R., and W. E. Seyfried (1986), Hydrothermal serpentinization of peridotite within the oceanic crust: Experimental investigations of mineralogy and major element chemistry, *Geochim. Cosmochim. Acta, 50,* 1357-1378.

Jean-Baptiste, P., E. Fourre, J. L. Charlou, J. P. Donval, and A. Dapoigny (2008), Deepwater mantle ^{3}He plumes over the northern Mid-Atlantic Ridge (36°N – 40°N) and Azores Platform, *Geochem. Geophys. Geosyst.*, *9,* doi: org/10.1029/2007GC0001765.

Kamesh Raju, K. A., V. N. Kodagali, and H. Fujimoto (1998), Three dimensional gravity and magnetic studies over a segment of the Carlsberg Ridge, *35th Annual Convention and meeting on* Continental Margins of India- Evolution, Processes and Potentials, *Indian Geophysical Union*, held at NIO, Goa, 18-20 Nov., 1998, P29.

Kamesh Raju, K. A., A. K. Chaubey, D. Amarnath, and A. V. Mudholkar (2008), Morphotectonics of the Carlsberg Ridge between 62°20' and 66°20'E, northwest Indian Ocean, *Mar. Geol., 252,* 120-128.

Kawagucci, S., K. Okamura, K. Kiyota, U. Tsunogai, Y. Sano, K. Tamaki, and T. Gamo (2008), Methane, manganese, and helium-3 in newly discovered hydrothermal plumes over the Central Indian Ridge, 18°-20°S, *Geochem. Geophys. Geosyst.*, *9,* doi:10.1029/2008GC002082.

Kelley, D. S, J. A. Karson, D. K. Blackman, G. L. Früh-Green, D. A. Butterfield, M. D. Lilley, E. J. Olson, M. O. Schrenk, K. K. Roe, G. T. Lebon, P. Rivizzigno, and the AT3-60 Shipboard Party (2001), An off-axis hydrothermal vent field near the Mid-Atlantic Ridge at 30°N, *Nature, 412*, 145–49.

Lackschewitz, K. S., R. Botz, D. Garbe-Schönberg, J. Scholten, and P. Stoffers (2006), Mineralogy and geochemistry of clay samples from active hydrothermal vents off the north coast of Iceland, *Mar. Geol., 225,* 177–190.

Lupton, J. E. (1976), The ^{3}He distribution in deep water over the Mid-Atlantic ridge, *Earth Planet. Sci. Lett., 32,* 371-374.

Lupton, J. E., G. P. Klinkhammer, W. R. Normark, R. Haymon, K. C. Macdonald, R. F. Weiss, and H. Craig (1980), Helium and Manganese at the 21°N East Pacific Rise hydrothermal site, *Earth Planet. Sci. Lett., 50,* 115-127.

Lupton, J. E., J. R. Delaney, H. P. Johnson, and M. K. Tivey (1985), Entrainment and vertical transport of deep-ocean water by buoyant hydrothermal plumes, *Nature*, *316,* 621-623.

Lupton, J. E. (1998), Hydrothermal helium plumes in the Pacific Ocean, *J. Geophys. Res., 103,* 15853-15868.

Marbler, H., A. Koschinsky, T. Pape, R. Seifert, S. Weber, E. T. Baker, L. M. de Carvalho, and K. Schmidt (2010), Geochemical and physical structure of the hydrothermal plume at the ultramafic-hosted Logatchev hydrothermal field at 14°45′N on the Mid-Atlantic Ridge, *Mar. Geol., 271,* 187-197.

McKenzie, D. P., P. Molnar, and D. Davies (1970), Plate techtonics of the Red Sea and East Africa, *Nature, 226,* 243-248.

Mudholkar, A. V., V. N. Kodagali, K. A. KameshRaju, A. B. Valsangkar, G. H. Ranade, and N. V. Ambre (2002), Geomorphological and petrological observation along a segment of slow-spreading Carlsberg Ridge, *Current Sci., 82,* 982-989.

Mudholkar, A. V. et al., *MV Akademik Boris Petrov cruise, BPR-1 cruise report,* 22pp. NIO, Goa. 2009.

Murton, B. J., E. T. Baker, C. M. Sands, and C. R. German (2006), Detection of an unusually large hydrothermal event plume above the slow-spreading Carlsberg Ridge: NW Indian Ocean, *Geophys. Res. Lett., 33,* 1-5.

Nakamura, K., S. Veirs, C. P. Sarason, R. E. McDuff, F. Stahr, D. R. Yoerger, and A. M. Bradley (2000), Electrochemical signals in rising buoyant plumes and tidally oscillating plumes at the main Endeavour vent field, Juan de Fuca Ridge. *Eos Trans., 81(48),* AGU Fall Meet. Suppl., Abstract OS52I-05.

Ramirez-Llodra, E., T. Shank, and C. R. German (2007), Biodiversity and Biogeography of Hydrothermal Vent Species, *Oceanography, 20,* 30-41.

Ray, D., I. H. Mirza, L. Surya Prakash, S. Kaisary, Y. V. B. Sarma, B. R. Rao, Y. K. Somayajulu, R. K. Drolia, and K. A. KameshRaju (2008), Water column geochemical anomalies associated with the

remnants of a mega plume: A case study after CR-2003 hydrothermal event in Carlsberg Ridge, NW Indian Ocean, *Current Sci.*, *95,* 355-360.

Rona, P. A., L. Widenfalk, and K. Bostrom (1987), Serpentinized ultramafics and hydrothermal activity at the Mid-Atlantic Ridge crest near 15°N, *J. Geophys. Res., 92,* 1417-1427.

Rudnicki, M. D., R. H. James, and H. Elderfield (1994), Near-field variability of the TAG non-buoyant plume, 26°N., Mid-Atlantic Ridge, *Earth Planet. Sci. Lett., 127,* 1 -10.

Saager, P. M., H. J. De-Baar, and P. H. Burkill (1989), Manganese and iron in the Indian Ocean waters, *Geochim. Cosmochim. Acta, 53,* 2259-2267.

Schmidt, K., A. Koschinsky, D. Garbe-Schoenberg, L.M. De Carvalho and R. Seifert (2007), Geochemistry of hydrothermal fluids from the ultramafic-hosted Logatchev hydrothermal field, 15°N on the Mid-Atlantic Ridge: temporal and spatial investigation, *Chem. Geol., 242*, 1–21.

Seyfried Jr., W. E., N. J. Pester, K. Ding, and M. Rough (2011), Vent fluid chemistry of the Rainbow hydrothermal system (36°N, MAR): Phase equilibria and in situ pH controls on subseafloor alteration processes, *Geochim. Cosmochim. Acta, 75,* 1574-1593.

Srinivasan, A., Z. Top, P. Scholsser, R. Hohmann, M. Iskandarani, D. B. Olson, J. E. Lupton, and W. J. Jenkins (2004), Mantle ^{3}He distribution and deep circulation in the Indian Ocean, *J. Geophys. Res., 109,* C06012, doi: 10.1029/2003JC002028.

Thomson, R. E., J. R. Delaney, R. E. McDuff, D. R. Janecky, and J. S. McClain (1992), Physical Characteristic of the Endeavour Ridge hydrothermal plume during July 1988, *Earth Planet. Sci. Lett., 111,* 141-154.

Van Dover, C. L., S. E. Humphris, D. Fornari, C. M. Cavanaugh, R. Collier, S. K. Goffredi, J. Hashimoto, M. D. Lilley, A. L. Reysenbach, T. M. Shank, K. L. Von Damm, A. Banta, R. M. Gallant, D. Gotz, D. Green, J. Hall, T. L. Harmer, L. A. Hurtado, P. Johnson, Z. P. McKiness, C. Meredith, E. Olson, I. L. Pan, M. Turnipseed, Y. Won, C. R. Young III, and R. C. Vrijenhoek (2001), Biogeography and ecological setting of Indian Ocean hydrothermal vents, *Science, 294*, 818-823.

Van Dover, C. L., C. R. German, K. Speer, L. Parson, and R. Vrijenhoek (2002), Evolution and biogeography of deep-sea vent and seep invertebrates, *Science, 295*, 1253-1257.

Van Gosen, B. S., H. A., Lowers, S. J., Sutley, and C. A. Gent (2004), Using the geologic setting of talc deposits as an indicator of amphibole asbestos content, *Environ. Geol., 45,* 920–939.

Walker, S. L., E. T. Baker, J. A. Resing, K. Nakamura, and P. D. McLain (2007), A new tool for detecting hydrothermal plumes: An ORP Sensor for the PMEL MAPR, *Eos Trans. 88(52),* AGU Fall Meet. Suppl., Abst. V21D-0753.

Wetzel, L. R., and E. L. Shock (2000), Distinguishing ultramafic from basalt-hosted submarine hydrothermal systems by comparing calculated vent fluid compositions, *J. Geophys. Res.*, *105,* 8319-8340.

Young, C., and J. E. Lupton (1983), An ultratight fuid sampling system using cold-welded copper tubing, *Eos Trans., AGU, 64,* 735.

Figure captions:

Figure 1. Swath bathymetric map of the survey area over Carlsberg ridge modified after Kamesh Raju et al, 2008. (A) Map showing four ridge segments (I to IV) with different tectonic settings: transform fault (TF), fracture zone (FZ) and off-axial highs. Among the four segments, Segment I, III and IV have a mega-structure of ridge parallel off-axial highs and shallow rift valley, while Segment II is characterized with scattered smaller highs but a deep axial valley. Segment IV has an offset with a prominent transform fault. The square symbols denote the dredging locations; red indicates recovery of mantle rocks and green shows recovery of basalts (Kamesh Raju et al, 2008). During BPR-1 cruise in 2009 one more dredge location (3°41.5'N, 63°50E) on an off-axial high near CTD 26 was found with ultramafic outcrops [*Mudholkar et al.,* 2009]. (B) Enlarged seafloor map of Segment II. The pink lines indicate deep tow (DT) tracks. The water column within the box (black dashed line) in Segment II was explored extensively.

Figure 2. Schematic diagram showing the array of six MAPRs attached along the cable used during the deep-tow survey. The IMI-30 system was towed at altitudes ranging from 400 to 500 m above the seafloor and thus three MAPRs attached below the depressor acquired near-bottom water column data. During the deep-tow survey, ship speed was maintained at 2.0 knots.

Figure 3. Bathymetric map of a portion of Segment II showing two deep-tow tracks (DT-04 and DT-06, pink lines). Pink circles show the CTD stations of the first expedition (S6 to S10 and S14 to S17) onboard *RV Sonne* (2007-cruise) and yellow diamonds show MAPR hydrocast locations for the water column survey during the second expedition onboard *MV Akademik Boris Petrov* (2009-cruise).

Figure 4. Optical backscatter anomaly (ΔNTU) profiles for the CTD hydrocast stations S6, S8, S9 and S10. The hydrothermal plume layers are shown by the arrows.

Figure 5. Contour plots showing the optical backscatter signature obtained from four MAPRs attached with DT-06. Black dotted lines show the tracks of four MAPRs with respect to the seafloor. The tracks of MAPR-5 and MAPR-6 are not shown in this plot. The indentified backscatter layer has a maximum ΔNTU $\geq$0.03. The vertical black lines show the CTD hydrocast (S16 and S17 of 2007 cruise) locations.

Figure 6. Vertical profiles of $\Delta\theta$ (A and E), ΔNTU (B and F), δ^3He (C and G) and dissolved Mn (D and H) against water depths at CTD station, S16 and S17. The profiles reveal a 200-250 m thick anomalous

layer of higher temperature, ΔNTU, excess δ^3He(%) and dissolved manganese within the water column between 2950 and 3200 m.

Figure 7. Plot of (A) potential temperature θ versus potential density σ_θ and (B) θ versus salinity in deep water (depth >2750 m) at the CTD station, S17. In these plots the effluent layer is marked by excess σ_θ and salinity of water between 3040 and 3190 m, relative to linear trends in ambient seawater above and below the same layer.

Figure 8. Six selected Scanning Electron Microscope (SEM) images (A-F) of filtered particulates in seawater collected from the backscatter layer (depth 3060m) at the CTD station, S17. The chemical composition of each particles determined with EDS are shown in the table below. ND= Not detectable.

Figure 9. Vertical MAPR profiles of in situ temperature (red line), ΔNTU (blue line) and E (green line) at four stations (8, 9, 24 and 32) from the 2009 cruise near CTD S17.

Figure 10. Vertical MAPR profiles for in situ temperature (red line), ΔNTU (blue line) and E (green line) at MAPR stations 36, 37, 38 and 39 from the 2009 cruise.

Figure 11. Vertical MAPR profiles for in situ temperature (red line), ΔNTU (blue line) and E (green line) at MAPR station 26 from the 2009 cruise.

Figure 1

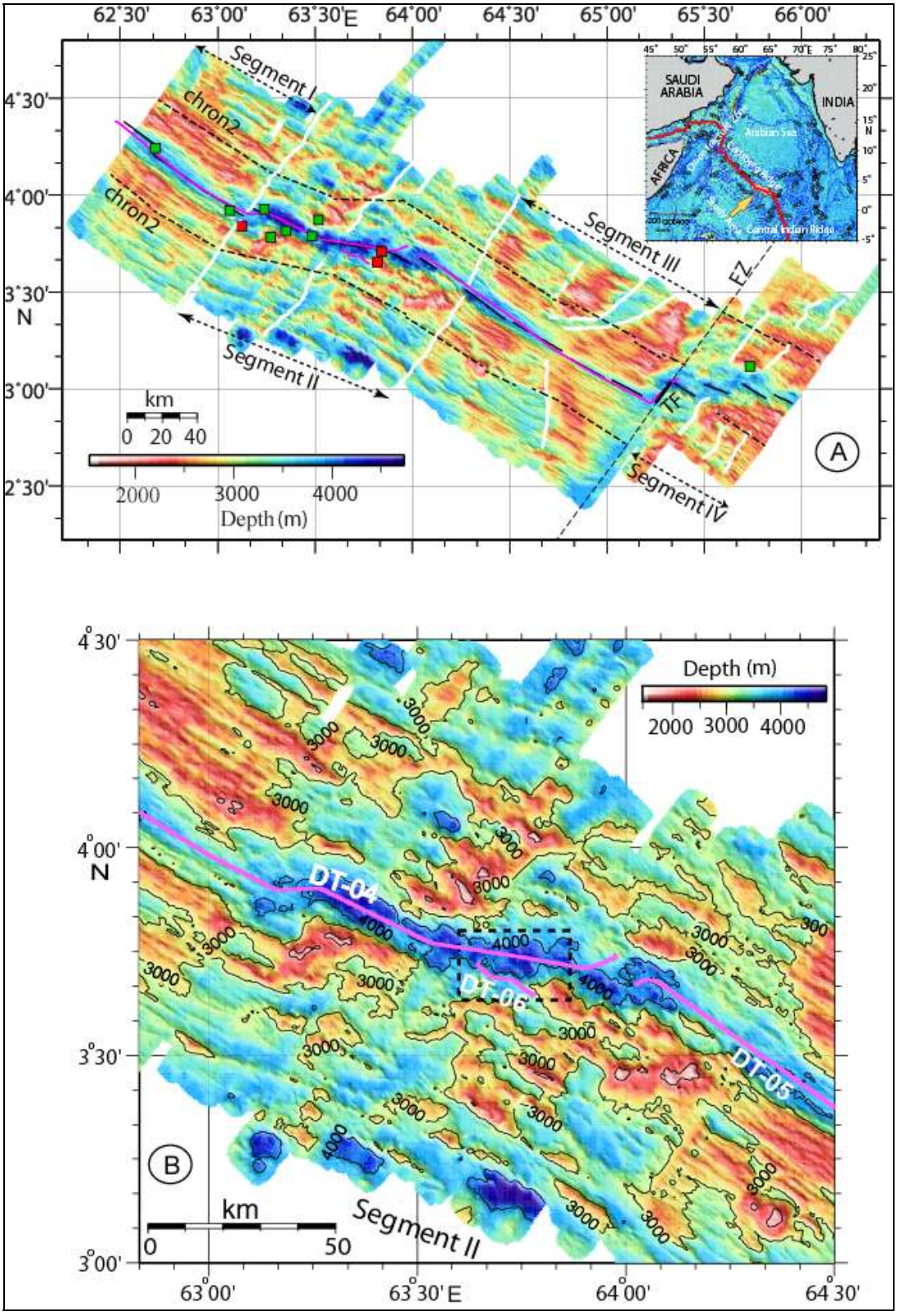
62°30'
63°00'
63°30'E
64°00'
64°30'
65°00'
65°30'
66°00'
4°30'
4°00'
3°30'
N
3°00'
2°30'
Segment I
chron2
chron2
Segment II
Segment III
FZ
TF
Segment IV
km
0 20 40
2000
3000
4000
Depth (m)
A
SAUDI ARABIA
INDIA
AFRICA
Arabian Sea
Central Indian Ridge
4°30'
4°00'
N
3°30'
3°00'
Depth (m)
2000 3000 4000
DT-04
DT-06
DT-05
B
km
0
50
Segment II
63°00'
63°30'E
64°00'
64°30'

Figure 2

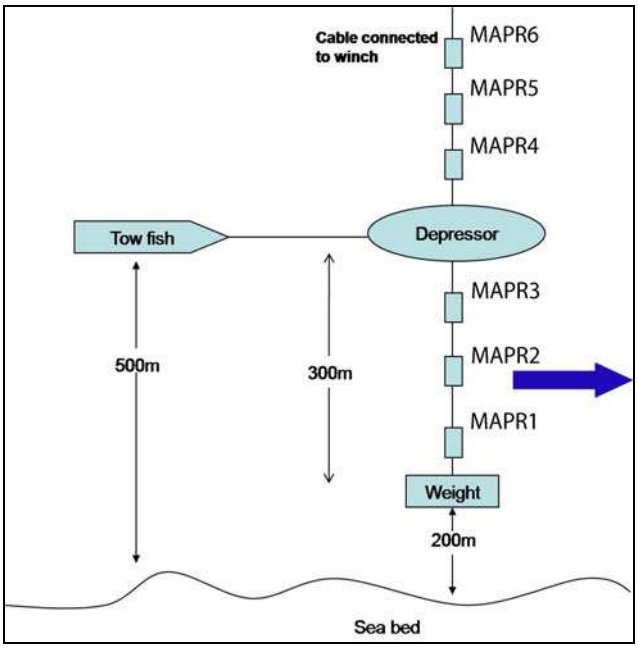

Figure 3

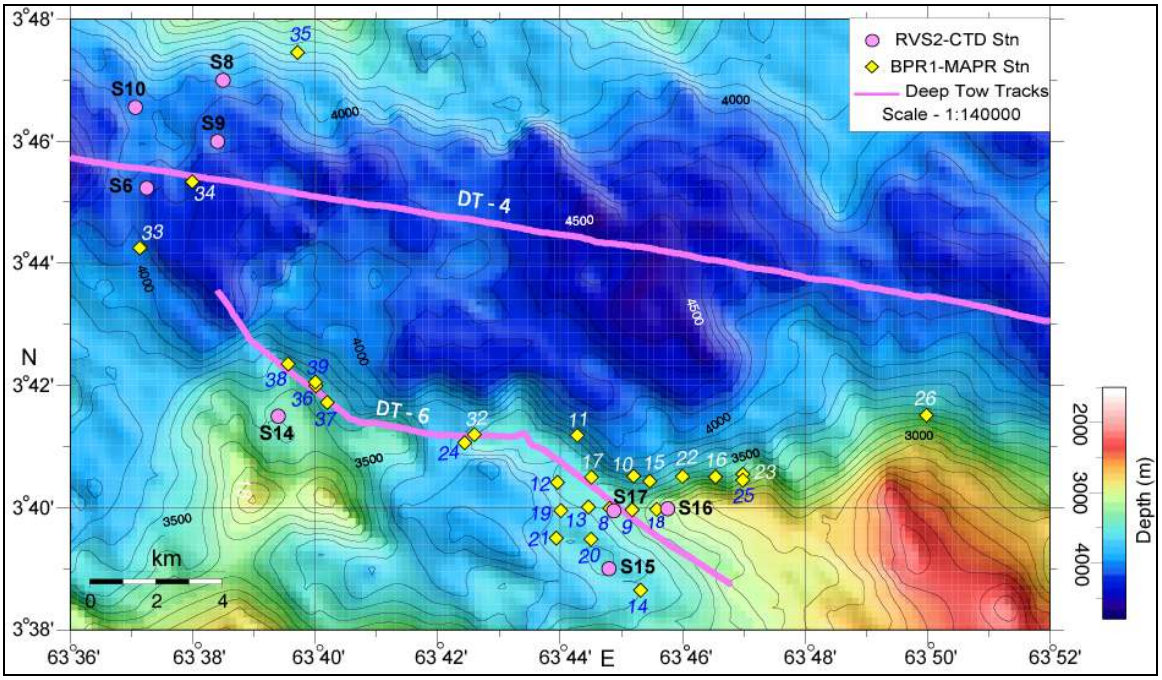

Figure 4

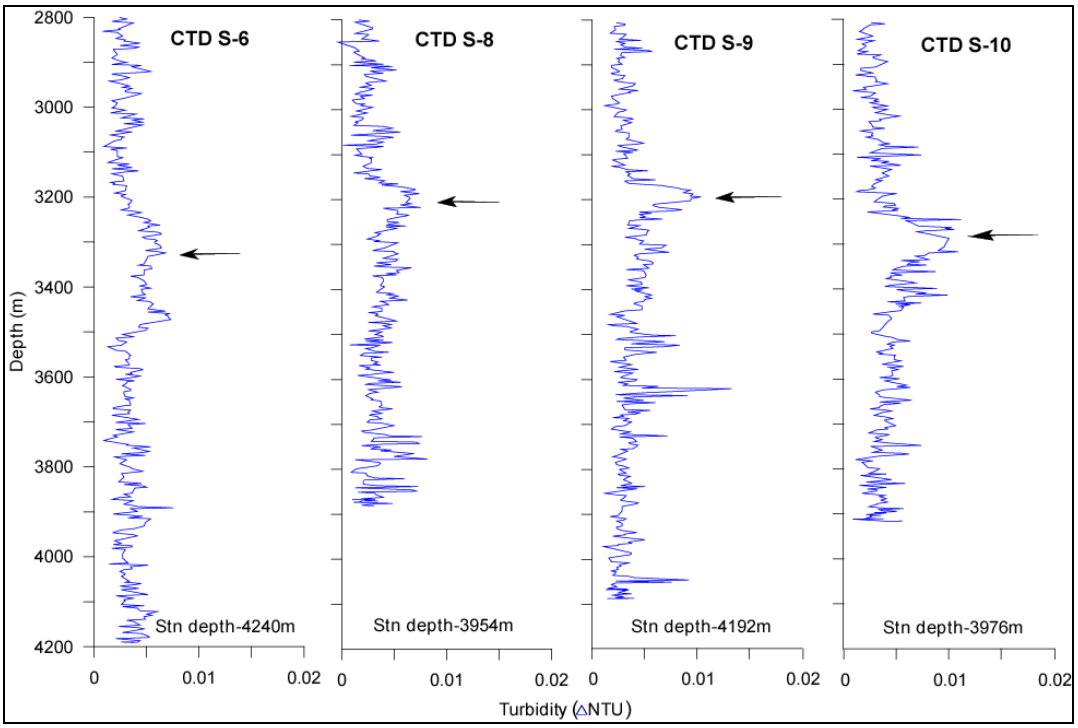

Figure 5

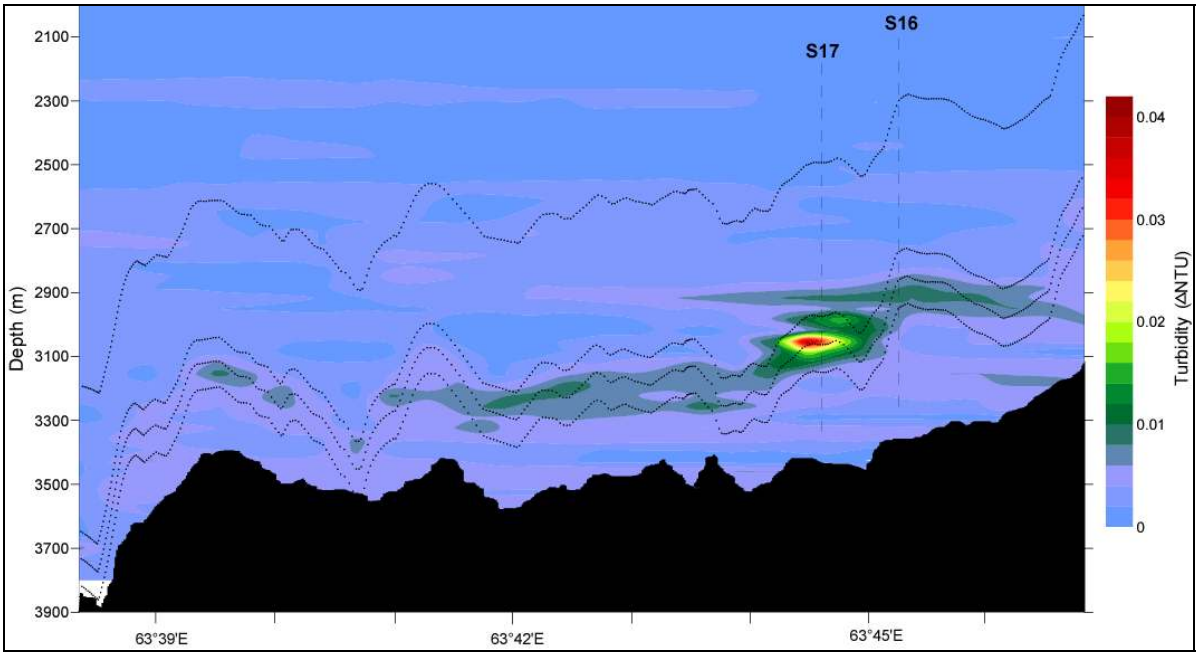

Figure 6

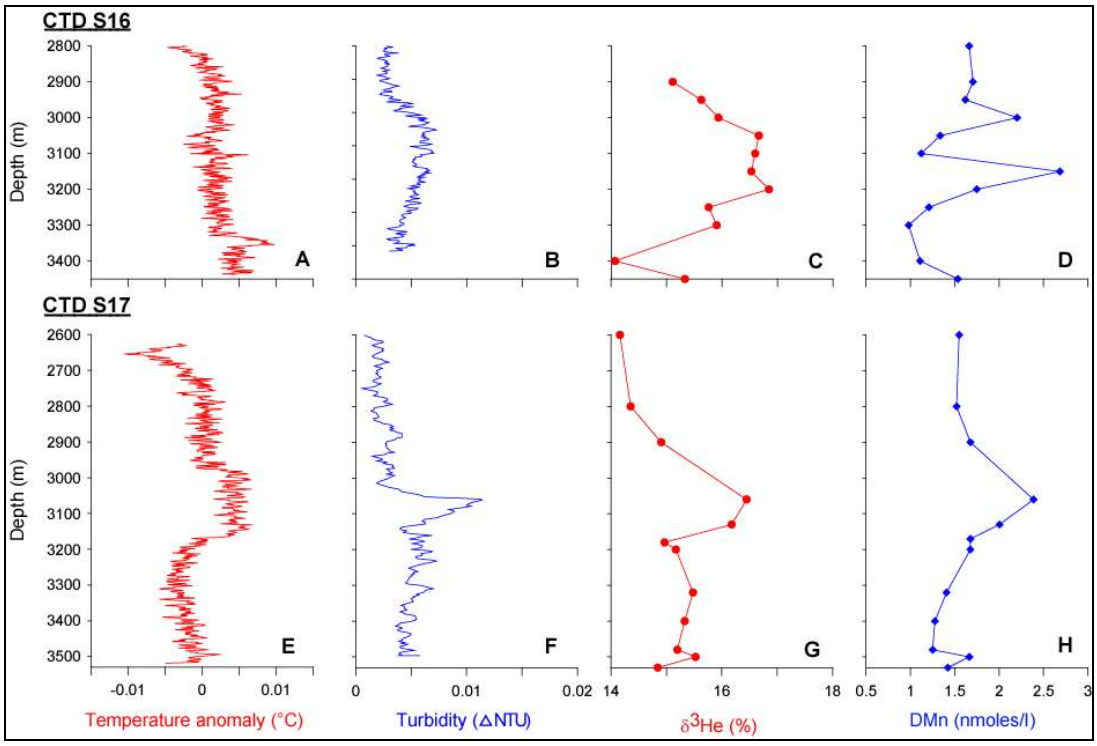

Figure 7

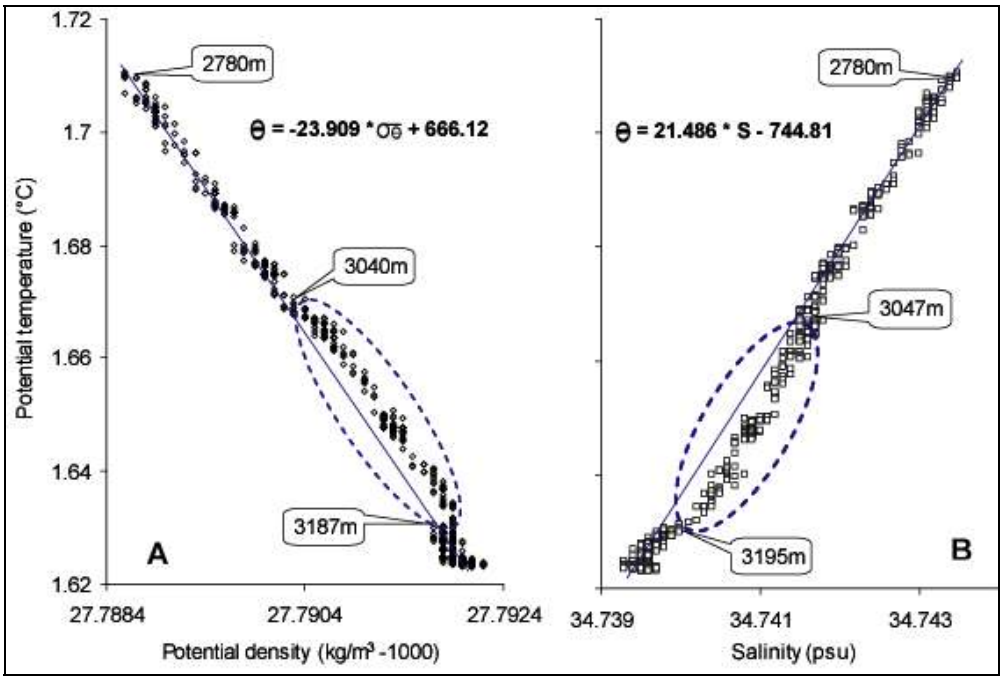

Figure 8

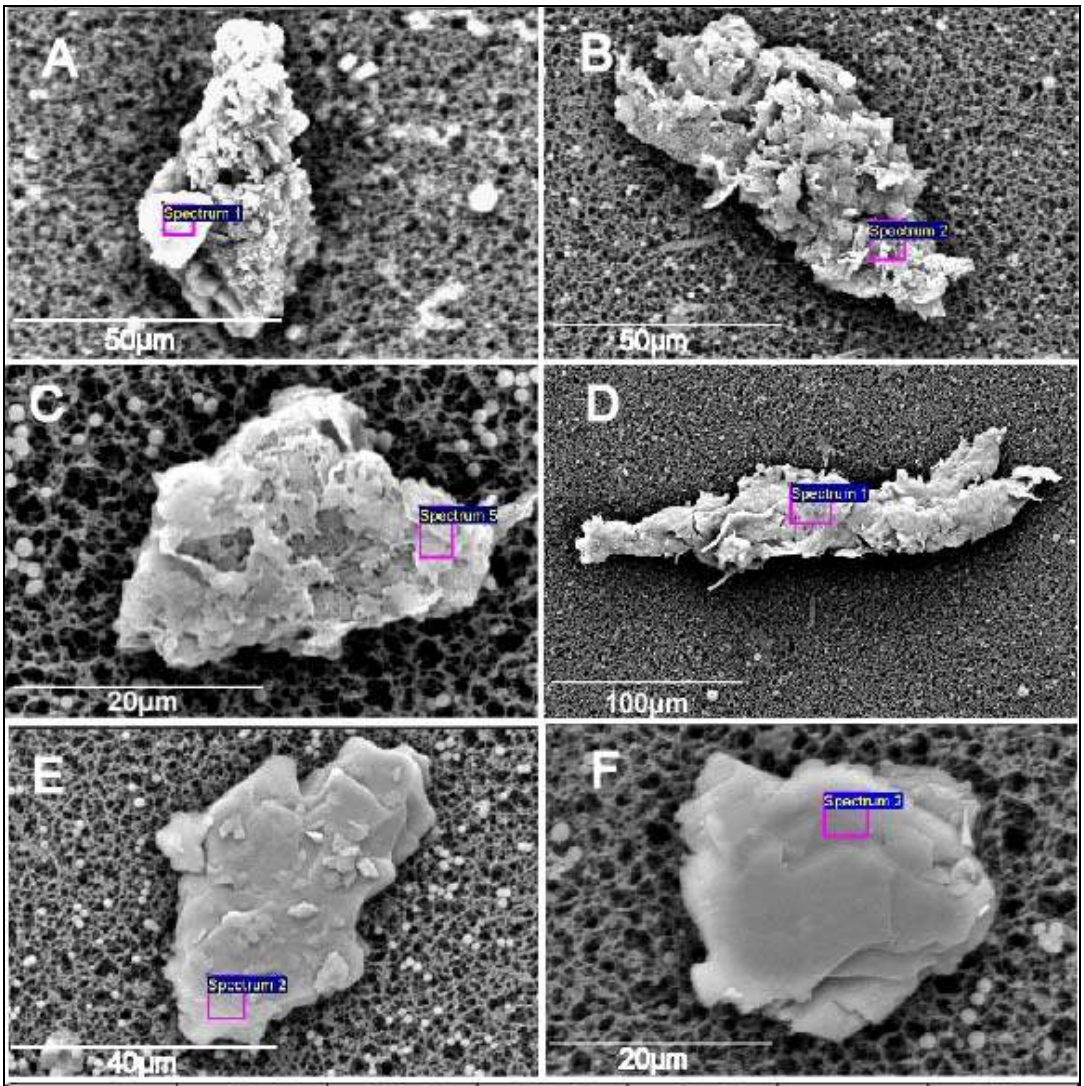

Comp.(%)	FeO	MnO	MgO	CaO	Al_2O_3	SiO_2
A	15.6	1.04	3.11	1.08	13.6	48.9
B	14.9	ND	1.37	1.03	1.84	71.2
C	11.9	ND	ND	1.21	1.97	75.5
D	8.89	ND	1.24	1.42	1.75	74.3
E	0.86	ND	33.0	ND	8.76	57.3
F	0.41	ND	31.3	ND	ND	68.2

Figure 9

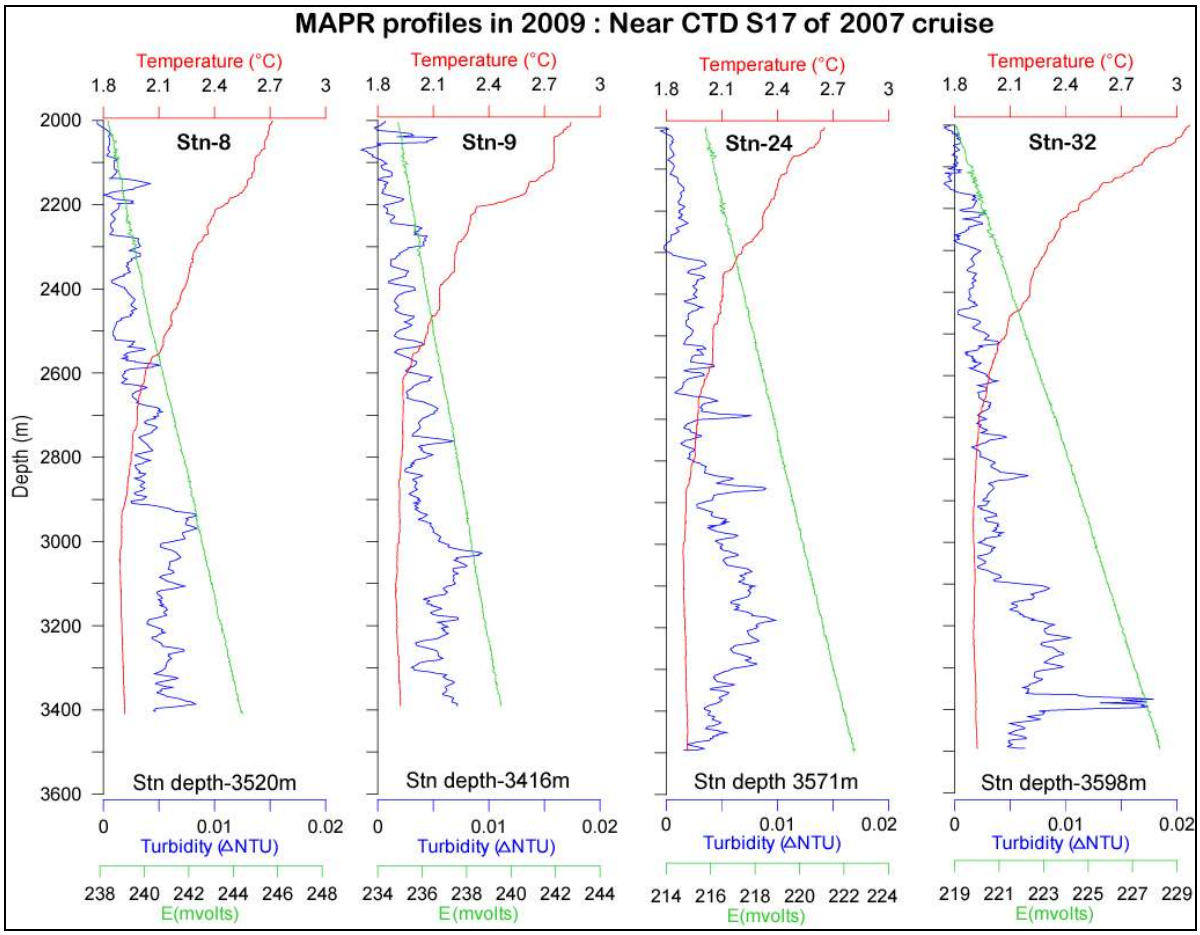
MAPR profiles in 2009 : Near CTD S17 of 2007 cruise
Temperature (°C)
1.8 2.1 2.4 2.7 3
Stn-8
Stn-9
Stn-24
Stn-32
Depth (m)
2000 2200 2400 2600 2800 3000 3200 3400 3600
Stn depth-3520m
Stn depth-3416m
Stn depth 3571m
Stn depth-3598m
0 0.01 0.02
Turbidity (ΔNTU)
238 240 242 244 246 248
234 236 238 240 242 244
214 216 218 220 222 224
219 221 223 225 227 229
E(mvolts)

Figure 10

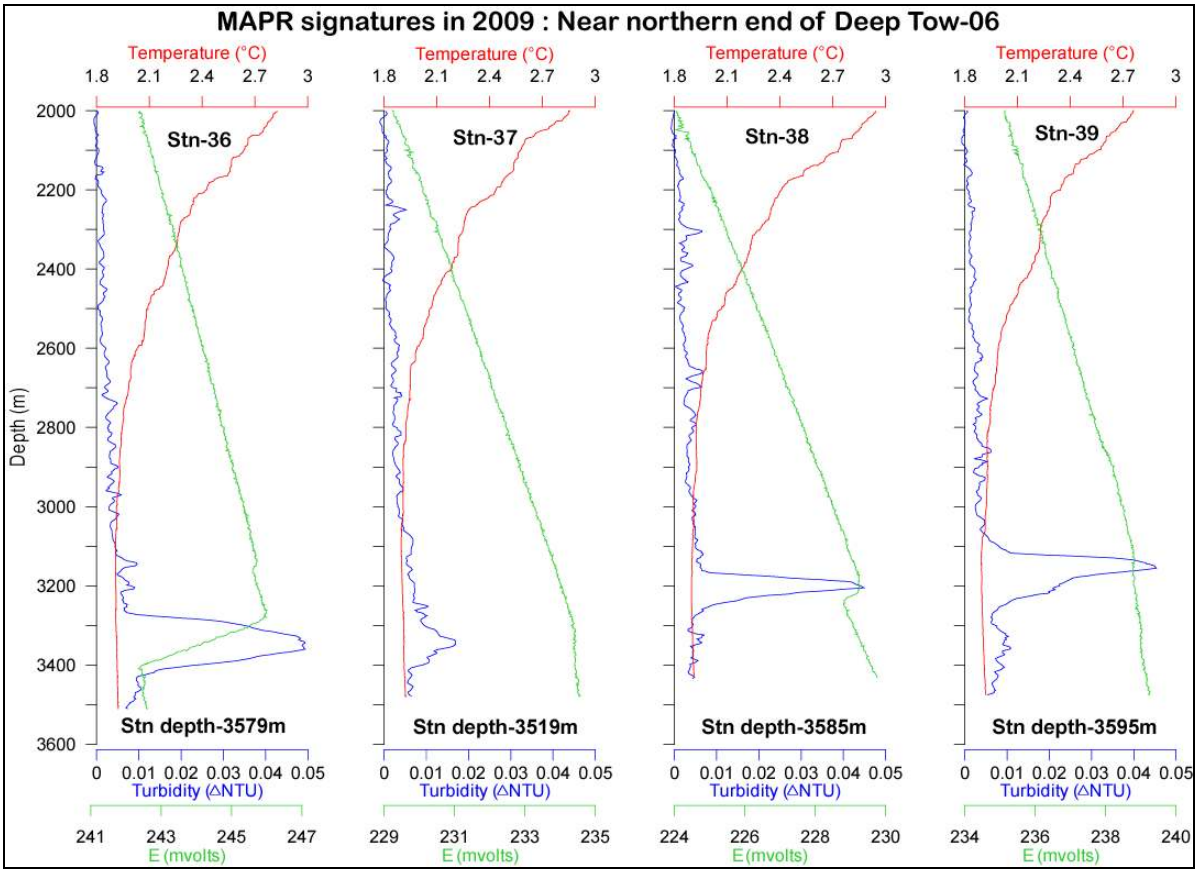
MAPR signatures in 2009 : Near northern end of Deep Tow-06
Temperature (°C)
1.8 2.1 2.4 2.7 3
Depth (m)
2000 2200 2400 2600 2800 3000 3200 3400 3600
Stn-36
Stn-37
Stn-38
Stn-39
Stn depth-3579m
Stn depth-3519m
Stn depth-3585m
Stn depth-3595m
0 0.01 0.02 0.03 0.04 0.05
Turbidity (ΔNTU)
241 243 245 247
229 231 233 235
224 226 228 230
234 236 238 240
E (mvolts)

Figure 11

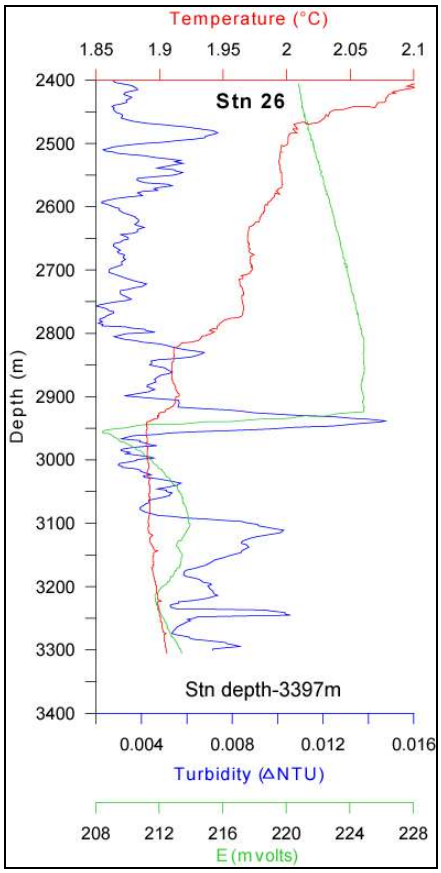
Temperature (°C)
1.85
1.9
1.95
2
2.05
2.1
Stn 26
Depth (m)
2400
2500
2600
2700
2800
2900
3000
3100
3200
3300
3400
Stn depth-3397m
0.004
0.008
0.012
0.016
Turbidity (ΔNTU)
208
212
216
220
224
228
E (mvolts)

Table 1: *Locations, date of operation and water column depths of (A) CTD stations of RVS-2 and (B) MAPR-hydrocast stations of BPR-1 cruises.*

CTD/MAPR station	Date	Latitude (N)	Longitude (E)	Depth (m)
A. CTD stations of the first expedition onboard *RV Sonne*				
S6	04.11.2007	03°45.23	63°37.25	4240
S8	04.11.2007	03°47.00	63°38.58	3954
S9	05.11.2007	03°46.01	63°38.50	4192
S10	05.11.2007	03°46.55	63°37.06	3976
S14	11.11.2007	03°41.50	63°39.40	3398
S15	11.11.2007	03°39.00	63°44.80	3606
S16	11.11.2007	03°40.01	63°45.59	3292
S17	12.11.2007	03°40.00	63°44.80	3553
B. MAPR stations of the second expedition onboard *MV Akademik Boris Petrov*				
8	11.05.2009	03°39.98	63°44.81	3554
9	15.05.2009	03°39.97	63°45.57	3416
24	17.05.2009	03°41.06	63°42.44	3581
26	17.05.2009	03°41.51	63°49.98	3429
32	20.05.2009	03°41.19	63°42.60	3615
36	21.05.2009	03°41.99	63°40.01	3585
37	22.05.2009	03°41.72	63°40.22	3529
38	22.05.2009	03°42.05	63°40.00	3585
39	22.05.2009	03°41.88	63°39.99	3612

Table 2: *Properties of seawater sample from the CTD stations S16 and S17. The shaded portions indicate the anomalous data correspond to the plume layer.*

Depth (m)	Potential temperature (^{o}C)	Salinity (psu)	δ^{3}He (%)	DMn (nmoles/l)
CTD S16				
2800	1.697	34.7428	--	1.66
2900	1.673	34.7419	15.11	1.7
2950	1.668	34.742	15.62	1.61
3000	1.663	34.7412	15.94	2.21
3050	1.661	34.7407	16.67	1.33
3100	1.658	34.7404	16.6	1.12
3150	1.630	34.74	16.53	2.68
3200	1.635	34.7398	16.85	1.74
3250	1.634	34.74	15.76	1.20
3300	1.633	34.7401	15.9	0.98
3400	1.626	34.7397	14.07	1.09
3450	1.624	34.7396	15.33	1.52
CTD S17				
2600	1.813	34.748	14.16	1.54
2800	1.705	34.7431	14.35	1.52
2900	1.676	34.7421	14.9	1.67
3060	1.649	34.7408	16.45	2.38
3130	1.634	34.7405	16.17	2.0
3180	1.629	34.7399	14.97	1.67
3200	1.627	34.7398	15.17	1.68
3320	1.624	34.7394	15.48	1.41
3400	1.623	34.7396	15.33	1.27
3480	1.623	34.7397	15.19	1.25
3500	1.622	34.7395	15.5	1.66
3530	1.621	34.7394	14.84	1.42